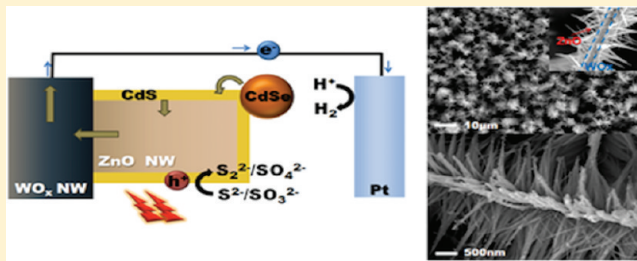


Highly Efficient Photoelectrochemical Hydrogen Generation Using Hierarchical ZnO/WO_x Nanowires Cosensitized with CdSe/CdS

Heejin Kim, Minsu Seol, Junghan Lee, and Kijung Yong*

Surface Chemistry Laboratory of Electronic Materials (SCHEMA), Department of Chemical Engineering, Pohang University of Science and Technology (POSTECH), Pohang 790-784, Korea

ABSTRACT: A photoelectrochemical device with a novel hierarchical heterostructure coupled with narrow bandgap semiconductors is demonstrated for efficient hydrogen generation via water splitting. The heterostructures consist of ZnO nanowire branches grown on WO_x nanowhisker stems, which offer a large surface area and efficient charge transport path. The assembly of CdSe/CdS narrow bandgap cosensitizers on hierarchical ZnO/WO_x nanostructures is shown to enhance light harvesting in the visible light region. The cosensitized ZnO/WO_x heterostructures demonstrate efficient light absorption up to a wavelength of 800 nm as well as enhanced photoelectrochemical properties when used as photoanodes. Furthermore, CdSe/CdS cosensitized ZnO/WO_x has a type II cascade band structure, resulting in efficient charge transport, which was confirmed by open circuit voltage decay measurements. Our photoelectrochemical system produced a high photocurrent density of 11 mA/cm² at -0.5 V (vs SCE) under 1.5 AM irradiation for hydrogen generation.



INTRODUCTION

One-dimensional nanostructures have been intensively investigated and applied as the nanoscale building blocks for the fabrication of various nanodevices because of their high surface-to-volume ratio, high aspect ratio, and the quantum confinement effect.^{1–5} These geometric properties provide a direct electron path and high electron mobility for efficient electronic devices; in addition, one-dimensional nanostructures can serve as promising photoanodes for effective photogenerated electron–hole pair diffusion.^{6–9} Because of these characteristics, the application of one-dimensional nanostructures as photoanodes in photoelectrochemical systems has been extensively studied over the past decades. This application generally requires the low recombination of electron–hole pairs, fast diffusion for efficient photo-induced performance, and effective light harvesting.^{10–12} In addition to this trend, the integration of one-dimensional nanostructures into three-dimensional nanostructure assemblies consisting of complex materials has also been intensively studied in recent years.^{13,14} In three-dimensional nanostructures, various properties with multifunctionality resulting from their morphological, multicomponent characteristics could be observed and utilized. Even more, the large surface area arising from this hierarchical structure is noteworthy and is very useful for creating an efficient architectural design in various applications, including photoelectrochemical or photocatalytic devices.

Recently, hydrogen generation has attracted much attention because of its importance in green energy development.^{15–17} One of the widely used methods for hydrogen generation is water photoelectrolysis using semiconductor materials or their multi-components as photoanodes in a photoelectrochemical system.^{18,19}

As a typical photoanode material, n-type wide bandgap semiconductors with various nanostructures have been utilized because of their photoelectrolytic properties.²⁰ However, their limited light absorption properties (confined to the UV region) degrade their water-splitting performance under solar light illumination. As a result, the coupling of a narrow bandgap semiconductor with a wide bandgap semiconductor has been attempted as a way to enhance photoelectrochemical efficiencies in visible-light-driven hydrogen generation. In many previous studies, the synthesis and application of multicomponent nanostructures assembled with narrow/wide-bandgap semiconductors have been widely investigated.^{21–23} One useful method is to deposit narrow-bandgap nanomaterials in the form of quantum dots or as a film to modify wide-bandgap semiconductors. Wang et al. reported a double-sided ZnO nanowire structure modified by low-bandgap semiconductor materials (CdS, CdSe) applied to a hydrogen generation system.²¹ Another type of low-bandgap semiconductor, CuInS₂, has also been deposited on TiO₂ nanoparticles, showing enhanced photoelectrochemical performance because of its enhanced visible light absorption property and reduced recombination through its appropriate conduction band position.²³ In addition to these materials, other types of narrow bandgap semiconductors (mostly in the form of quantum dots) have been studied as sensitizers for efficient photoelectrochemical cells.^{24–26}

Tungsten oxide (WO_x) is a well-known photoanode material useful for the photoelectrolysis of water. The hierarchical nanostructure

Received: September 27, 2011

Revised: November 8, 2011

Published: November 16, 2011

of WO_x also has potential as a promising photoanode because of its high surface area and multifunctionality. Hierarchical heteronanostructures consisting of WO_x nanowhiskers and ZnO nanowires have been synthesized by depositing ZnO on the surface of WO_x nanowhiskers. Uniformly deposited needle-type ZnO nanowires on WO_x nanowhiskers can offer a high aspect ratio and large surface area.²⁷ On the basis of this hierarchical heteronanostructure, we modified the ZnO/WO_x hierarchical nanostructure by depositing low-bandgap semiconductor materials (CdSe/CdS) for photoelectrochemical hydrogen generation applications. In our system, the WO_x core nanowhisker acts as a charge transport material, with a low electrical resistivity of $1.75 \times 10^{-3} \Omega \text{ cm}$.²⁸ It also acts as a scaffold for ZnO nanowire growth. In addition, deposited ZnO nanowires on WO_x nanowhiskers serve as wide-bandgap semiconductors that can photosensitize UV irradiation. Although this pristine ZnO/WO_x hierarchical nanostructure can be applied as a photoanode for a photoelectrochemical cell, it primarily utilizes the UV region. Thus, for enhanced light absorption in the visible light region, narrow-bandgap semiconductors (CdSe/CdS) were coupled to the hierarchical nanowires by deposition of these materials using successive ionic layer adsorption and reaction (SILAR) and chemical bath deposition (CBD) processes. The deposited low-bandgap semiconductor facilitates enhanced light harvesting. Another important point is that the composite multicomponent of $\text{CdSe}/\text{CdS}/\text{ZnO}/\text{WO}_x$ has a type II cascade band-alignment structure that is useful for efficient charge transport. These effects result in enhanced photoelectrochemical performance. In short, we fabricated a ZnO/WO_x hierarchical heteronanostructure modulated by low-bandgap semiconductor sensitizers (CdSe/CdS) with the aims of (i) extending the light absorption range into the visible light regime, (ii) reducing the recombination of electron/hole pairs by cascade electron transport, and (iii) increasing the surface area for more efficient photoelectrochemical hydrogen generation. These novel hierarchical heteronanostructures provide a high photocurrent density of 11 mA/cm^2 in our photoelectrochemical system, which ensures a highly enhanced conversion efficiency in hydrogen generation.

■ EXPERIMENTAL SECTION

Synthesis of ZnO/WO_x Heteronanostructures. Growth of ZnO/WO_x heterostructures was performed using a simple two-step method.²⁷ WO_x nanowhiskers were first synthesized using a conventional two-zone horizontal tube furnace and the thermal evaporation of WO_3 powder. A W substrate, cleaned with acetone, was placed on top of an alumina boat containing the WO_3 powder (Aldrich, 99%) and then positioned in the center of the furnace. After the chamber was evacuated to the vacuum level (50–100 mTorr), the temperature was slowly increased to the growth temperature (1050 °C) and then maintained for 1 h. After the growth process, the furnace was allowed to naturally cool back to room temperature. Subsequently, for ZnO growth, a ZnO seed layer was sputter-deposited using a ZnO target at room temperature. After that, the WO_x nanowhiskers deposited with the ZnO seed layer were immersed in a 10 M $\text{Zn}(\text{NO}_3)_2 \cdot 6\text{H}_2\text{O}$ solution, wherein the pH was adjusted by the addition of an ammonia solution. The hydrothermal synthesis of ZnO nanowires was conducted at 95 °C for 6 h. After growth, the substrates were removed from the solution, rinsed with deionized water, and dried using nitrogen gas.

Deposition of a Low Bandgap Semiconductor (CdSe/CdS) onto ZnO/WO_x Heteronanostructures. For the deposition of CdS and CdSe , solution-reaction growth was conducted under different reaction conditions. First, CdS was coated on the surface of the ZnO nanowires using the SILAR method at room temperature. The ZnO/WO_x heteronanostructures were dipped into a 100 mM CdSO_4 aqueous solution and subsequently into a 100 mM Na_2S aqueous solution at room temperature. The CdS shell layer thickness was controlled by the number of SILAR cycles. Subsequently, CdSe deposition was carried out at 95 °C using the CBD process. To nucleate of CdSe quantum dots onto the $\text{CdS}/\text{ZnO}/\text{WO}_x$ heteronanostructures, the sample was immersed in a solution containing 2.5 mM $\text{Cd}(\text{CH}_3\text{COO})_2$, 2.5 mM Na_2SeSO_3 , and 45 mM NH_4OH for 3 h. The size of the CdSe nanoparticles was controlled by the number of CBD reaction cycles.²⁹

Characterization. Scanning electron microscopy (SEM) images were taken using a Phillips XL30S field emission SEM. Transmission electron microscopy (TEM) analysis was performed on a transmission electron microscope (JEM-2100F, JEOL) equipped with an energy-dispersive X-ray (EDX) spectrometer. The optical absorbance of the samples was analyzed using a UV2501PC (SHIMADZU) spectrometer with an ISR-2200 integrating sphere attachment for diffuse reflection measurements. Photocurrent–voltage (I – V) measurements were performed using a typical three-electrode potentiostat system (potentiostat/galvanostat, model 263A, EG&G Princeton Applied Research) with a Pt counter electrode and a saturated calomel reference electrode (SCE). An aqueous solution containing 0.25 M Na_2S and 0.35 M Na_2SO_3 was used as the electrolyte through which nitrogen was bubbled, and the working electrode was illuminated from the front side with a solar-simulated light source (AM 1.5 G filtered, 100 mW/cm², 91160, Oriel).

■ RESULTS AND DISCUSSION

Fabrication of Hierarchical ZnO/WO_x Nanostructure and Deposition of CdSe/CdS . Figure 1 depicts SEM images showing the morphological changes of the hierarchical ZnO/WO_x nanostructure upon subsequent deposition of CdS and CdSe . Figure 1a shows the pristine hierarchical ZnO/WO_x nanostructures grown on the W substrate, which was prepared by the hydrothermal growth of ZnO nanowires onto WO_x nanowhiskers. As shown in the inset, the ZnO nanowires were grown as nanobranches on the WO_x nanowhiskers surface. After 6 h of growth, highly dense, uniform ZnO nanowire branches were found on the WO_x nanowhisker stem surface that were 20–50 nm in diameter and ~2 μm in length (Figure 1b). The SILAR process was conducted using a 0.1 M solution of the cation (CdSO_4) and anion (Na_2S) source for CdS deposition onto the ZnO nanowire surface. Subsequently, CdSe deposition was carried out by the CBD process at 95 °C. As the deposition progressed, the color of the samples changed from gray to dark brown. In addition, SEM analysis was conducted to examine the surface morphological changes, and surface modification is confirmed in Figure 1c,d. After the CdS deposition, the ZnO nanowires became thicker, and the surface became rough, as observed in the SEM image in Figure 1c. After the SILAR growth of CdS , the ZnO nanowires had a tendency to gather and form nanowire bunches. Subsequent CBD of CdSe yielded uniformly deposited CdSe nanoparticles on the $\text{CdS}/\text{ZnO}/\text{WO}_x$ nanostructures, as observed in Figure 1d.

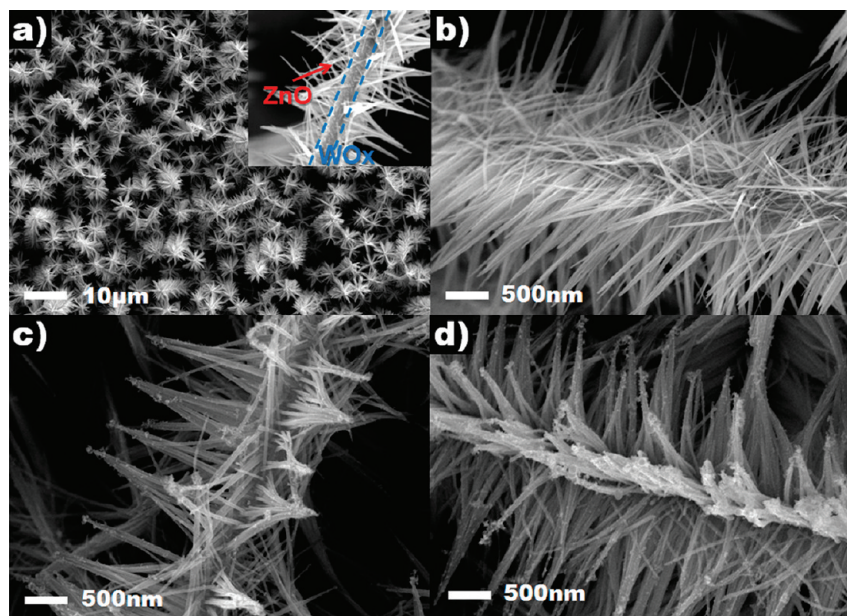


Figure 1. SEM images of the hierarchical heterostructure consisting of ZnO nanowires on WO_x nanowhiskers: (a) low magnification top view and (b) high magnification image (6 h growth condition). The inset in (a) depicts the initial stage growth sample. High magnification SEM images of (c) CdS-coated ZnO/ WO_x and (d) CdSe/CdS/ZnO/ WO_x .

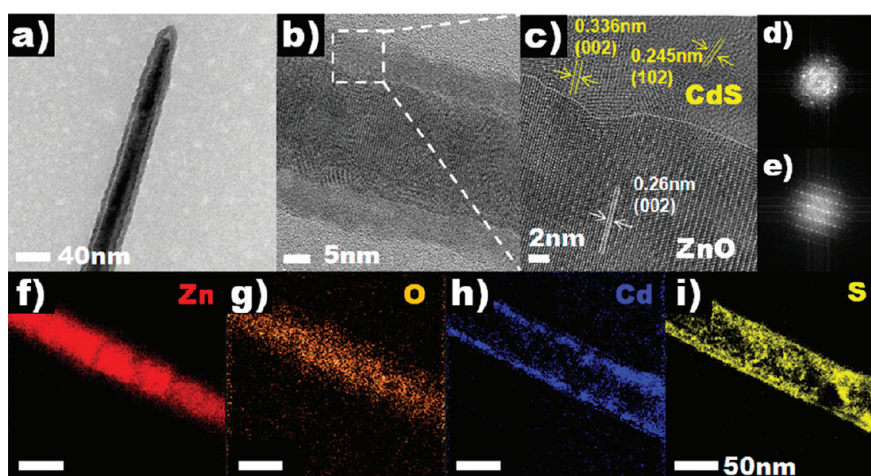


Figure 2. TEM analysis of ZnO/ WO_x heterostructures coated with CdS, focusing on CdS/ZnO at (a) low magnification and (b) high magnification. (c) HRTEM image of the corresponding sample of (b), and (d,e) FFT patterns of the CdS and ZnO obtained from (c). (f–i) EELS elemental mapping images of Zn, O, Cd, and S, respectively.

To obtain a better understanding of the detailed surface morphology changes and characteristics, we carried out a TEM analysis, which confirmed the subsequent growth of CdS and CdSe onto the ZnO nanowire surfaces. After the SILAR process for the CdS shell coatings, thin CdS shell layers on the ZnO nanowire surface could be observed (Figure 2). After 20 cycles of the SILAR process, a highly uniform CdS thin shell layer was deposited onto the ZnO nanowire core with a 6–7 nm shell thickness consisting of polycrystalline nanostructures. The atomic structure of the ZnO/CdS core/shell nanowire was studied using high-resolution TEM (HRTEM). The HRTEM images confirmed polycrystalline atomic arrangements of a CdS coating on a single-crystal ZnO core nanowire grown along the (0001) direction. Fast Fourier transform (FFT) patterns taken from the core/shell parts also

confirmed the presence of the crystal structures of ZnO/CdS core/shell nanowires. The CdS shell layer thickness can be controlled by the number of SILAR cycles.⁶ Spatial elemental analysis using electron energy loss spectroscopy (EELS) was also performed (Figure 2f–i), and the results confirmed that the CdS shell was coated on the ZnO nanowire core. While Zn and O atoms were found on the nanowire core, Cd and S elements were mainly observed on the shell portion of the core/shell nanowires.

After CdS deposition, CBD was performed for the deposition of CdSe. As observed in the SEM analysis results, the nanowire surface became rough and bumpy as a result of the CBD process. The CdSe deposited onto the CdS/ZnO/ WO_x structure was also examined using TEM, and the images are shown in Figure 3. Figure 3a presents a low-magnification TEM image of the CdSe

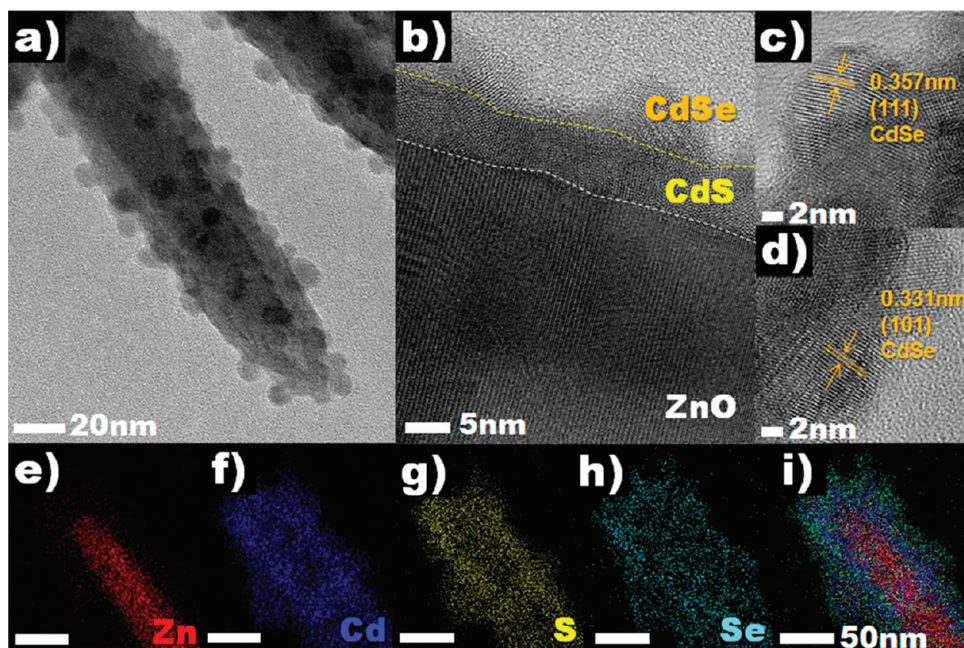


Figure 3. TEM analysis of CdS/ZnO/WO_x heterostructures coated with CdSe at (a) low magnification and (b–d) HRTEM images of CdSe/CdS coupled with ZnO nanowire. (e–h) EDS elemental mapping analysis of Zn, Cd, S, and Se, respectively, and (i) EDS overlay image of images e–h.

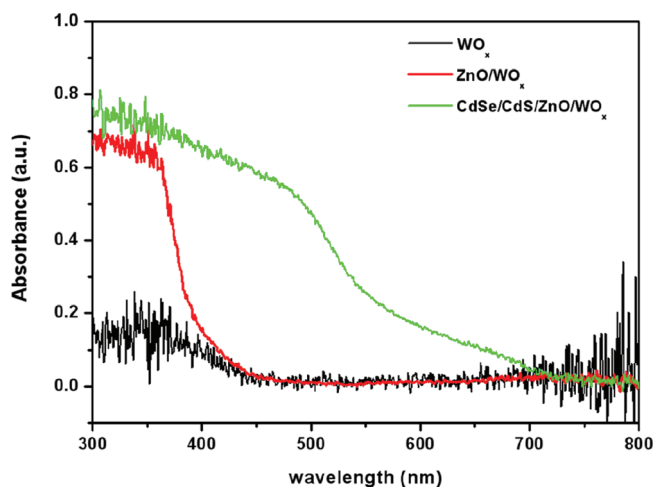


Figure 4. Diffused reflectance absorption spectra of (black) WO_x nanowhiskers on W substrate, (red) ZnO/WO_x heterostructures prepared by the two-step process, and (green) ZnO/WO_x nanostructures coated with CdSe/CdS prepared using SILAR and CBD processes.

deposited sample, which clearly displays uniformly deposited CdSe nanoparticles on the ZnO nanowires coated with a CdS shell. High-resolution TEM revealed polycrystalline CdSe nanoparticles with an average diameter of ~ 6.5 nm (Figure 3b–d). In addition, EDS mapping images (Figure 3e–i) indicate that the CdSe nanoparticles were uniformly deposited on the ZnO/CdS core/shell nanowires. On the basis of the surface analysis results using SEM and TEM, we conclude that nano-CdSe/CdS modified hierarchical ZnO/WO_x nanostructures could be fabricated using a series of step processes.

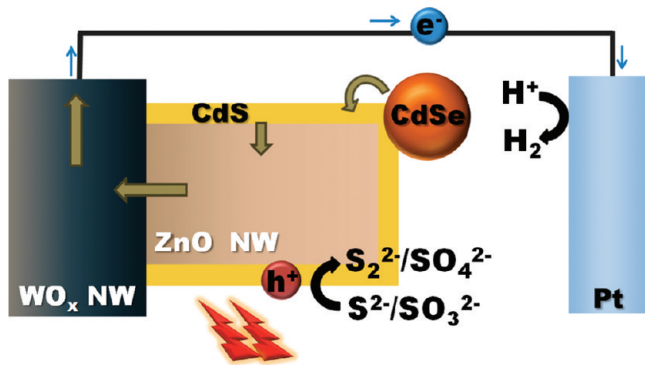
Optical and Photoelectrochemical Properties of CdSe/CdS/ZnO/WO_x Nanostructures. Because ZnO has a wide bandgap (3.2 eV), it has been studied as a promising photoanode that absorbs UV region wavelengths. However, because of its limited

light absorption range, the photoelectrochemical performance of ZnO alone is relatively poor. Similar to ZnO, WO₃ is a widely used material for photoelectrochemical hydrogen generation. However, WO₃ also has a relatively wide bandgap and an indirect bandgap, resulting in a relatively low absorption coefficient. In the present work, we have fabricated hierarchical ZnO/WO_x nanostructures and applied this novel heteronanostructure as a photoanode for photoelectrochemical hydrogen generation. To enhance light harvesting in the visible light region, CdSe/CdS cosensitization was employed by modifying the hierarchical ZnO/WO_x nanostructures with the deposition of CdSe/CdS nano-materials. Tungsten suboxide (WO_{3-x}, 0 < x < 1) has relatively high electron mobility (W₁₈O₄₉ NW, 40 cm² V⁻¹ s⁻¹; WO₃, 6.5 cm² V⁻¹ s⁻¹). Thus, in our system, WO_x acts as a charge transport material for the photogenerated electrons in CdSe/CdS/ZnO, which has a type II band alignment structure.

To examine the optical properties of the prepared samples, diffused reflectance spectra were studied, as observed in Figure 4. In Figure 4, the black line obtained from pristine WO_x shows very weak absorption in the UV region, and the red line originating from ZnO/WO_x shows strong absorption for light wavelengths below ~ 400 nm. The addition of CdSe/CdS to ZnO/WO_x widens the light absorption range in the visible light region up to a wavelength of ~ 800 nm. The reason for this enhanced visible light absorption is the low bandgap properties (CdS, 2.4 eV; CdSe, 1.7 eV). Absorption edges are observed at 530 nm (2.35 eV) for CdS and at 700 nm (1.77 eV) for CdSe.³⁰

Using these CdSe/CdS sensitized hierarchical ZnO/WO_x nanostructures as photoanodes, we studied their photoelectrochemical properties for hydrogen generation. To investigate the photoelectrochemical performance, we employed a CdSe/CdS/ZnO/WO_x nanostructure grown on a W substrate as the photoanode in a three-electrode PEC system. Scheme 1 illustrates a schematic diagram of the CdSe/CdS/ZnO/WO_x PEC cell with sacrificial reagent electrolytes and the mechanism of hydrogen generation in our system. Under irradiation, photogenerated

Scheme 1. Schematic Diagram of the PEC System Based on CdSe/CdS/ZnO/WO_x with the Overall Reaction Mechanism



electrons in the narrow bandgap semiconductor (CdSe, CdS) are injected into the conduction band of ZnO, while the remaining holes in the cathode oxidize the S²⁻ ions into S₂²⁻ ions. Through the cascaded band position of the electrodes, electrons pass through CdSe/CdS/ZnO/WO_x to the W substrate and transfer to the Pt counter electrode. The electrons at the Pt counter electrode were consumed to reduce H⁺ to H₂. The sacrificial reagent in the electrolyte (SO₃²⁻) acts as a hole scavenger by preventing a back reaction by reducing S₂²⁻ to S²⁻. This explains the basic mechanism for photoelectrochemical hydrogen generation in our system.^{25,31}

Figure 5a is a set of chopped sweep current density versus potential curves from various NW photoanodes using white light illumination of 100 mW/cm² (AM 1.5G). Four types of NW photoanodes were studied, and their PEC performance was compared: WO_x nanowhiskers, a ZnO/WO_x hierarchical nanostructure, a CdS sensitized ZnO/WO_x hierarchical nanostructure, and a CdSe/CdS cosensitized ZnO/WO_x hierarchical nanostructure. The SILAR cycle number of CdS deposition was optimized to 20 cycles in photocurrent study. Also, the CBD process for CdSe deposition was repeated three times, subsequently. A 20 cycle number of SILAR generated the maximized photocurrent density. In the case of the WO_x nanowhiskers photoanode, negligible photocurrent generation is observed, which we believe is due to the inefficient light absorption property of the WO_x nanowhiskers, as seen in the UV-vis spectra. The ZnO/WO_x hierarchical nanostructure showed a slightly enhanced photocurrent because of the enhanced light absorption of ZnO in the UV region. As compared to pristine ZnO/WO_x, the CdS and CdSe/CdS sensitized hierarchical ZnO/WO_x nanostructures showed drastically increased photocurrent density, which results from the enhanced light harvesting in the visible light region and the efficient charge transport through the stepwise band structure. In particular, the CdSe/CdS cosensitized hierarchical sample exhibited the highest photocurrent density among the four samples. The photocurrent density was saturated at near -0.7 V (vs SCE), and a maximum photocurrent of 11 mA/cm² at -0.5 V bias vs SCE was achieved for the 6–7 nm CdS shell thickness and CdSe nanoparticles with an average of ~6.5 nm. The photocurrent density obtained in our study is comparable to other narrow-bandgap semiconductor sensitized structures studied by other researchers, who reported photocurrent density ranging from 0.35 to 17.4 mA/cm².^{22,23,25,26,29,32–34} These results imply that heterojunctioned CdSe/CdS structures provide considerable synergy effects for light harvesting, enhancing charge transport and reducing recombination.

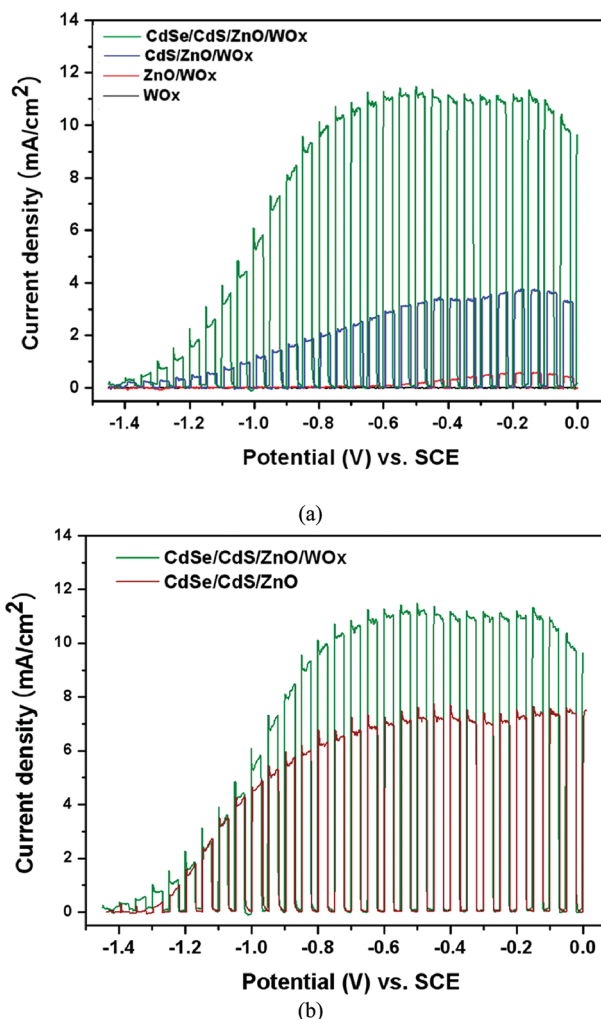


Figure 5. (a) Chopped illumination (100 mW/cm²) current density versus potential (*J*–*E*) characteristics of (black) as-prepared WO_x nanowhiskers, (red) ZnO/WO_x, (blue) CdS/ZnO/WO_x, and (green) CdSe/CdS/ZnO/WO_x. (b) Comparison *J*–*E* curves under chopped illumination with (a) CdSe/CdS/ZnO/WO_x and (b) CdSe/CdS/ZnO.

In our system, the wide-bandgap semiconductor consists of ZnO nanowires and WO_x nanowhiskers. As described in the previous section, the WO_x nanowhiskers act as the charge transport material having semimetal properties as well as the scaffold for ZnO nanowire growth. To better understand the role of the WO_x nanowhiskers in the PEC performance, we prepared two different photoanode samples and compared their PEC results: a CdSe/CdS cosensitized hierarchical ZnO/WO_x nanostructure and CdSe/CdS cosensitized ZnO nanowires. The ZnO nanowire growth was carried out under equal reaction conditions (6 h ammonia solution growth), and CdS/CdSe deposition was conducted at the same deposition cycles. The photocurrent density versus applied voltage results obtained from the two samples is shown in Figure 5b. Figure 5b shows that the cosensitized ZnO/WO_x has a higher photocurrent density as compared to the cosensitized ZnO nanowires. The enhanced PEC performance from the hierarchical sample is due to the higher density of ZnO nanowires grown on WO_x nanowhiskers as compared to those grown on a flat substrate, which results in a higher coverage of sensitizers on the nanowires. These results support our conclusion that our hierarchical nanostructures

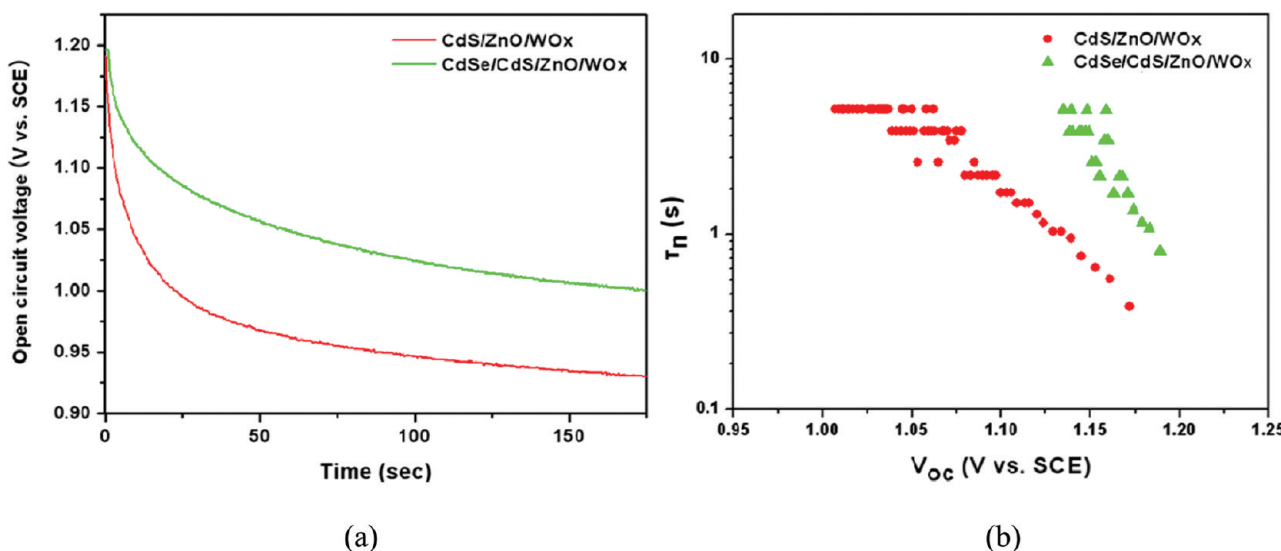


Figure 6. (a) Open circuit voltage decay with time for the CdS/ZnO/WO_x and CdSe/CdS/ZnO/WO_x photoelectrodes after illumination interruption. (b) Electron lifetime derived from the given equation as a function of V_{oc} .

can make very useful photoanodes in a PEC system for hydrogen generation.

Open circuit voltage measurements were performed to examine the effective charge transport and recombination lifetime. In our system, CdSe/CdS cosensitization plays a very important role in both visible light absorption and charge transport because of the type II band alignment structure. Although CdS and CdSe have a type I band structure in a bulk system, they are known to have a type II band structure in a junction system because of Fermi level alignment.³⁵ When CdSe/CdS are coupled on the ZnO surface, they have more negative conduction bands, which are beneficial for hydrogen generation, and their cascade band structure is advantageous for efficient electron transport. Because of these effects, the cosensitized CdSe/CdS hierarchical nanostructure showed relatively high PEC performance as compared to CdS- or CdSe-only sensitized nanostructures. Analysis of the open circuit voltage decay showed that the CdSe/CdS coupled heterostructure alleviated open circuit voltage decay as compared to the CdS coupled sample (Figure 6a). These results indicate that the CdSe/CdS structure efficiently enhances charge transport with an appropriate conduction band position and also reduces electron recombination. We have examined the recombination kinetics by calculating the voltage–recombination lifetime. The model equation follows:³⁶

$$\tau_n = -\frac{k_B T}{e} \left(\frac{dV_{oc}}{dt} \right)^{-1}$$

where k_B is Boltzmann's constant, T is the temperature, V_{oc} is the open circuit voltage, and e is the elementary charge.³⁷ The calculated results showed that the CdSe/CdS cosensitized photoanode exhibited a higher electron lifetime with a lower recombination rate as compared to the CdS-only sensitized sample, as shown in Figure 6b. We believe that this phenomenon originates from efficient charge separation/transport through the cascade conduction band position, known as type II band alignment.

In addition, we measured the stability of the PEC performance along with its time dependence. Figure 7 demonstrates the photoresponse of the CdSe/CdS/ZnO/WO_x, CdS/ZnO/WO_x,

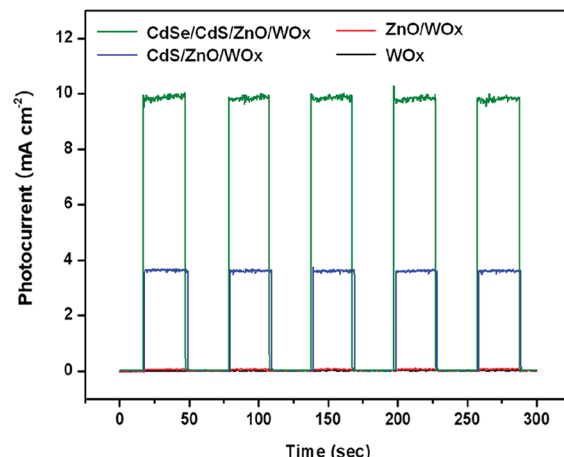
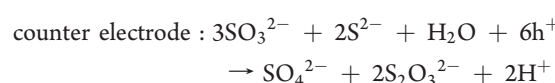


Figure 7. Current–time ($I-t$) measurement of (green) CdSe/CdS/ZnO/WO_x, (blue) CdS/ZnO/WO_x, (red) ZnO/WO_x, and (black) WO_x at a bias of -0.7 V (vs SCE).

ZnO/WO_x and WO_x photoelectrodes carried out using a potentiostatic measurement at -0.7 V (vs SCE). Because the measured photocurrent was saturated near -0.7 V, we examined the photocurrent density at -0.7 V with time dependence under intermittent illumination. The photocurrent density with time was highly stable for all samples tested at the repeated illumination.

On the basis of the photoelectrochemical hydrogen generation mechanism, the photogenerated electrons and holes both contribute to the water splitting. Although the electrolyte used in the PEC experiment is a sacrificial reagent, the generated electrons and holes can generally participate in water splitting. In the case of our photoelectrodes, the hydrogen generation proceeds as follows:^{25,31}



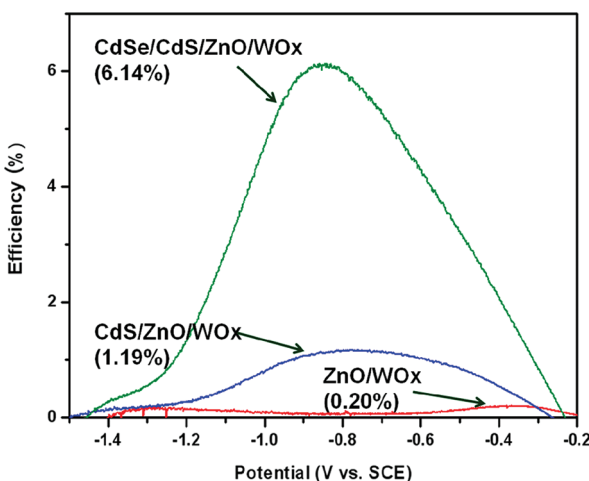


Figure 8. Light-to-chemical energy conversion efficiency of the CdSe/CdS/ZnO/WO_x, CdS/ZnO/WO_x, and ZnO/WO_x photoelectrodes obtained at an illumination of 100 mW cm⁻².

The overall reaction results in hydrogen generation by consuming the sacrificial reagent rather than water splitting. The calculated conversion efficiency can be overestimated as compared to the case of water splitting, which also accompanies oxygen generation. In Figure 8, we compare the conversion efficiency of hydrogen generation for three different samples: hierarchical ZnO/WO_x nanostructures, CdS sensitized ZnO/WO_x, and CdSe/CdS cosensitized ZnO/WO_x. The conversion efficiency calculation was performed using the following equation:³⁸ $n_c\text{ (\%)} = [(\text{energy converted to chemical reactions} - \text{energy supplied by external bias})/\text{energy of incident light}] \times 100$.

$$n_c\text{ (\%)} = \left[\frac{J_p(\Delta G^\circ_{\text{rev}} - E_{\text{bias}})}{J_0} \right] \times 100$$

where $\Delta G^\circ_{\text{rev}}$ is the Gibbs free energy per coulomb of electrons for the redox reactions at the electrodes, J_p is the photocurrent density, and J_0 is the intensity of the incident light (100 mW cm⁻²). The calculated efficiency showed that the CdSe/CdS cosensitized heteronanostructure has the highest conversion efficiency of 6.14% at -0.84 V, which is highly enhanced as compared to the efficiency of the pristine ZnO/WO_x heterostructure of 0.20% at -0.36 V. Although the conversion efficiency we obtained is overestimated because of the sacrificial reagent electrolyte, this value is relatively high as compared to other narrow-bandgap semiconductor coupled nanostructures.^{25,32,39}

CONCLUSION

In summary, we developed CdSe/CdS cosensitized hierarchical ZnO/WO_x nanostructured photoelectrodes for efficient PEC hydrogen generation. Hierarchical ZnO/WO_x nanostructures provided effective charge collection paths, and CdSe/CdS cosensitizers enhanced visible light harvesting. The type II band alignment of CdSe/CdS/ZnO/WO_x ensures efficient charge transport with a high electron lifetime, as confirmed by open circuit voltage decay measurements. The synthesized CdSe/CdS/ZnO/WO_x photoelectrodes produced a high photocurrent density of 11 mA/cm² at -0.5 V bias vs SCE for hydrogen generation. These results indicate that our novel hierarchical nanostructures are promising photoanode materials for PEC applications.

AUTHOR INFORMATION

Corresponding Author

*E-mail: kyong@postech.ac.kr.

REFERENCES

- (1) Cui, Y.; Lieber, C. M. *Science* **2001**, *291*, 851.
- (2) Gudiksen, M. S.; Lauhon, L. J.; Wang, J.; Smith, D. C.; Lieber, C. M. *Nature* **2002**, *415*, 617.
- (3) Yang, P.; Yan, H.; Mao, S.; Russo, R.; Johnson, J.; Saykally, R.; Morris, N.; Pham, J.; He, R.; Choi, H. J. *Adv. Funct. Mater.* **2002**, *12*, 323.
- (4) Boukai, A. I.; Bunimovich, Y.; Tahir-Kheli, J.; Yu, J. K.; Goddard III, W. A.; Heath, J. R. *Nature* **2008**, *451*, 168.
- (5) Baxter, J. B.; Aydil, E. S. *Appl. Phys. Lett.* **2005**, *86*, 053114.
- (6) Leschkies, K. S.; Divakar, R.; Basu, J.; Enache-Pommer, E.; Boercker, J. E.; Carter, C. B.; Kortshagen, U. R.; Norris, D. J.; Aydil, E. S. *Nano Lett.* **2007**, *7*, 1793.
- (7) Liu, B.; Aydil, E. S. *J. Am. Chem. Soc.* **2009**, *131*, 3985.
- (8) Hwang, Y. J.; Boukai, A.; Yang, P. *Nano Lett.* **2008**, *9*, 410.
- (9) Xu, F.; Dai, M.; Lu, Y.; Sun, L. *J. Phys. Chem. C* **2010**, *114*, 2776.
- (10) Shankar, K.; Basham, J. I.; Allam, N. K.; Varghese, O. K.; Mor, G. K.; Feng, X.; Paulose, M.; Seabold, J. A.; Choi, K. S.; Grimes, C. A. *J. Phys. Chem. C* **2009**, *113*, 6327.
- (11) Maiolo, J. R., III; Kayes, B. M.; Michael, A.; Putnam, M. C.; Kelzenberg, M. D.; Atwater, H. A.; Lewis, N. S. *J. Am. Chem. Soc.* **2007**, *129*, 12346.
- (12) Goodey, A. P.; Eichfeld, S. M.; Lew, K. K.; Redwing, J. M.; Mallouk, T. E. *J. Am. Chem. Soc.* **2007**, *129*, 12344.
- (13) Bierman, M. J.; Jin, S. *Energy Environ. Sci.* **2009**, *2*, 1050.
- (14) Shi, J.; Hara, Y.; Sun, C. L.; Anderson, M. A.; Wang, X. D. *Nano Lett.* **2011**, *11*, 3413.
- (15) Mor, G. K.; Shankar, K.; Paulose, M.; Varghese, O. K.; Grimes, C. A. *Nano Lett.* **2005**, *5*, 191.
- (16) Bak, T.; Nowotny, J.; Rekas, M.; Sorrell, C. C. *Int. J. Hydrogen Energy* **2002**, *27*, 991.
- (17) Younlpblood, W. J.; Lee, S. H. A.; Kobayashi, Y.; Hernandez-Pagan, E. A.; Hoertz, P. G.; Moore, T. A.; Moore, A. L.; Gust, D.; Mallouk, T. E. *J. Am. Chem. Soc.* **2009**, *131*, 926.
- (18) Youngblood, W. J.; Lee, S. H. A.; Maeda, K.; Mallouk, T. E. *Acc. Chem. Res.* **2009**, *42*, 1966.
- (19) Mor, G. K.; Varghese, O. K.; Wilke, R. H. T.; Sharma, S.; Shankar, K.; Latempa, T. J.; Choi, K. S.; Grimes, C. A. *Nano Lett.* **2008**, *8*, 1906.
- (20) Mor, G. K.; Shankar, K.; Varghese, O. K.; Grimes, C. A. *J. Mater. Res.* **2004**, *19*, 2989.
- (21) Wang, G.; Yang, X.; Qian, F.; Zhang, J. Z.; Li, Y. *Nano Lett.* **2010**, *10*, 1088.
- (22) Hensel, J.; Wang, G. M.; Li, Y.; Zhang, J. Z. *Nano Lett.* **2010**, *10*, 478.
- (23) Li, T. L.; Lee, Y. L.; Teng, H. J. *Mater. Chem.* **2011**, *21*, 5089.
- (24) Zhang, F.; Maeda, K.; Takata, T.; Domen, K. *Chem. Commun.* **2010**, *46*, 7313.
- (25) Nagasuna, K.; Akita, T.; Fujishima, M.; Tada, H. *Langmuir* **2011**, *27*, 7294.
- (26) Chen, H. M.; Chen, C. K.; Chang, Y. C.; Tsai, C. W.; Liu, R. S.; Hu, S. F.; Chang, W. S.; Chen, K. H. *Angew. Chem.* **2010**, *49*, 5966.
- (27) Kim, H.; Jeon, S.; Lee, M.; Lee, J.; Yong, K. J. *Mater. Chem.* **2011**, *21*, 13458.
- (28) Viswanathan, K.; Brandt, K.; Salje, E. J. *Solid State Chem.* **1981**, *36*, 45.
- (29) Seol, M.; Kim, H.; Kim, W.; Yong, K. *Electrochim. Commun.* **2010**, *12*, 1416.
- (30) Seol, M.; Kim, H.; Tak, Y.; Yong, K. *Chem. Commun.* **2010**, *46*, 5521.
- (31) Ni, M.; Leung, M. K. H.; Leung, D. Y. C.; Sumathy, K. *Renewable Sustainable Energy Rev.* **2007**, *11*, 401.

- (32) Chi, C. F.; Lee, Y. L.; Weng, H. S. *Nanotechnology* **2008**, *19*, 125704.
- (33) Gao, X. F.; Sun, W. T.; Ai, G.; Peng, L. M. *Appl. Phys. Lett.* **2010**, *96*, 153104.
- (34) Sung, T. K.; Kang, J. H.; Jang, D. M.; Myung, Y.; Jung, G. B.; Kim, H. S.; Jung, C. S.; Cho, Y. J.; Park, J.; Lee, C.-L. *J. Mater. Chem.* **2011**, *21*, 4553.
- (35) Lee, Y. L.; Chi, C. F.; Liau, S. Y. *Chem. Mater.* **2009**, *22*, 922.
- (36) Zaban, A.; Greenshtein, M.; Bisquert, J. *ChemPhysChem* **2003**, *4*, 859.
- (37) Bisquert, J.; Fabregat-Santiago, F.; Mora-Seró, I. n.; García-Belmonte, G.; Giménez, S. *J. Phys. Chem. C* **2009**, *113*, 17278.
- (38) Bolton, J. R. *Solar Energy* **1996**, *57*, 37.
- (39) Shin, K.; Seok, S. I.; Im, S. H.; Park, J. H. *Chem. Commun.* **2010**, *46*, 2385.